Arteriosclerosis, Thrombosis, and Vascular Biology

BASIC SCIENCES

Magnetic Resonance Imaging Reveals Distinct Roles for Tissue Transglutaminase and Factor XIII in Maternal Angiogenesis During Early Mouse Pregnancy

Gadi Cohen,* Ron Hadas,* Rachele Stefania, Amerigo Pagoto, Shifra Ben-Dor, Fortune Kohen, Dario Longo, Michal Elbaz, Nave Dekel, Eran Gershon, Silvio Aime, Michal Neeman

OBJECTIVE: The early embryo implantation is characterized by enhanced uterine vascular permeability at the site of blastocyst attachment, followed by extracellular-matrix remodeling and angiogenesis. Two TG (transglutaminase) isoenzymes, TG2 (tissue TG) and FXIII (factor XIII), catalyze covalent cross-linking of the extracellular-matrix. However, their specific role during embryo implantation is not fully understood.

APPROACH AND RESULTS: For mapping the distribution as well as the enzymatic activities of TG2 and FXIII towards blood-borne and resident extracellular-matrix substrates, we synthetized selective and specific low molecular weight substrate analogs for each of the isoenzymes. The implantation sites were challenged by genetically modifying the trophoblast cells in the outer layer of blastocysts, to either overexpress or deplete TG2 or FXIII, and the angiogenic response was studied by dynamic contrast–enhanced-magnetic resonance imaging. Dynamic contrast–enhanced-magnetic resonance imaging revealed a decrease in the permeability of decidual vasculature surrounding embryos in which FXIII were overexpressed in trophoblast cell. Reduction in decidual blood volume fraction was demonstrated when either FXIII or TG2 were overexpressed in embryonic trophoblast cell and was elevated when trophoblast cell was depleted of FXIII. These results were corroborated by histological analysis.

CONCLUSIONS: In this study, we report on the isoenzyme-specific roles of TG2 and FXIII during the early days of mouse pregnancy and further reveal their involvement in decidual angiogenesis. Our results reveal an important magnetic resonance imaging-detectable function of embryo-derived TG2 and FXIII on regulating maternal angiogenesis during embryo implantation in mice.

VISUAL OVERVIEW: An online visual overview is available for this article.

Key Words: blood volume ■ embryo implantation ■ factor XIII ■ magnetic resonance imaging ■ transglutaminase

Implantation of mammalian blastocysts into the uterine endometrium involves a series of precisely synchronized events that are influenced by interactions between the embryo and its maternal environment.[1] On attachment, during the fifth day of mouse pregnancy,[2] the embryo invades the maternal uterine epithelium at the anti-mesometrial pole of the implantation site (IS).[3] Consequently, uterine stromal cells rapidly proliferate and differentiate to form the decidua,[4] providing a permissive and controlled environment for the invasion of embryonic trophoblast cells (TC).[5,6] Concurrently, maternal blood vessels expand in number and diameter, and uterine vascular permeability increases locally around the IS.[7,8] These changes enabled invasive detection of embryo IS at an early stage by leakage

See accompanying editorial on page 1507

Correspondence to: Michal Neeman, Department of Biological Regulation, Weizmann Institute of Science, Rehovot, 76100 Israel. Email michal.neeman@weizmann.ac.il
*G.C. and R.H. contributed equally.

The online-only Data Supplement is available with this article at https://www.ahajournals.org/doi/suppl/10.1161/ATVBAHA.119.312832.
For Sources of Funding and Disclosures, see page 1612.

Arterioscler Thromb Vasc Biol is available at www.ahajournals.org/journal/atvb

Nonstandard Abbreviations and Abbreviations

CIV	collagen IV
CRISPR	clustered regularly interspaced short palindromic repeats
DCE-MRI	dynamic contrast–enhanced-magnetic resonance imaging
DTPA	diethylenetriaminepentaacetic acid
ECM	extracellular-matrix
FXIII	factor XIII
GFP	green fluorescent protein
ICR	Institute of Cancer Research
IS	implantation site
LV	lentivirus
PS	permeability surface area product
SA	substrate analog
sgRNA	single guide RNA
TC	trophoblast cells
TFA	trifluoroacetic acid
TG	transglutaminase
TG2	tissue TG

of intravenously administered vital dyes, and noninvasive detection of embryo implantation by dynamic contrast–enhanced (DCE)-magnetic resonance imaging (MRI).[9,10]

Embryo implantation failure is the primary cause for the low rate of success of in vitro fertilization programs.[4] Impaired uterine hyperpermeability has been proposed as a cause for implantation failure in humans.[11] Several complications of pregnancy, such as preeclampsia and intrauterine growth restriction, have been attributed to disturbances in early uterine blood supply[12] or impaired TC invasion of the placental bed spiral arterioles later in pregnancy.[13] TGs (transglutaminases) catalyze covalent cross-links between proteins in various processes associated with angiogenesis and extracellular matrix remodeling, such as wound healing, cancer invasion, and embryo implantation.[14] The most prominent TG isoenzymes are TG2 (tissue TG), that serves as a signaling molecule aside from its cross-linking activity[15,16] and FXIII (factor XIII), which participates in the final stage of the coagulation cascade, by catalyzing cross-links between fibrinogen or fibrin molecules.[17,18] In addition to fibrinogen, several extracellular-matrix glycoproteins, such as collagen, were found to be cross-linked by FXIII.[19–21]

We previously reported substrate analogs (SAs) for both TG2 and FXIII, labeled with either Gd (III)-DTPA (diethylenetriaminepentaacetic acid) or DOTA (gadoterate meglumine) or a fluorescent dye were designed to investigate their role in mouse models of tumor xenografts and blood clotting.[22,23] Selective peptide substrates specific for either TG2 or FXIII were identified by a phage display screen.[24] Given that both TG2 and FXIII are expressed at the embryo-maternal surface during early development,[16,25] the aim of this study was to determine the distinct roles of TG2 and FXIII in maternal vascular development during embryo implantation in mice. To do so, we successfully synthesized SAs for the 2 enzymes[26,27] demonstrating a highly selective and specific reactivity to their respective TG isoenzymes. TG2 and FXIII activities were further confirmed by determining the synthetized SAs distributions on IS sections. The contribution of embryo-derived TG activity was assessed by genetically modifying the blastocyst trophectoderm, in which the outer TC underwent lentiviral infection to overexpress TG2 or FXIII or using CRISPR-CAS9 (clustered regularly interspaced short palindromic repeats-associated protein 9) endonuclease to deplete their expression.

Briefly, DCE-MRI of surrogate pregnant mice carrying embryos with FXIII overexpressed TC, revealed a significant decrease in blood volume at the IS regions, while reduction in vessel permeability was demonstrated in embryonic TC overexpressing either FXIII or TG2. Furthermore, IS with FXIII-depleted TC displayed a significant increase vascular permeability, while vasculature changes were not detected in IS of TG2-depleted embryos. These MRI results demonstrate the distinct roles of embryo-derived TG2 and FXIII in maternal vascular remodeling during embryo implantation.

Highlights

- TG2 (tissue TG) and FXIII (factor XIII) transglutaminases are active in the embryo implantation site in mice.
- Modulation of trophoblast TG2 or FXIII expression alters maternal angiogenesis.
- TG (transglutaminase) modulation maternal angiogenesis in implantation is detectable by magnetic resonance imaging.

MATERIALS AND METHODS

The data that support the findings of this study are available from the corresponding author on reasonable request.

Synthesis and Characterization of the SAs F11-B and T29-B

All materials were purchased from Sigma-Aldrich Israel Ltd, Rehovot, Israel unless indicated otherwise. T29: REQLYLYNVFS and F11: DQMMLPWPAVKL sequences were based on a phage-displayed random peptide library screen.[24,26,28] Peptides were synthetized by a Liberty CEM microwave peptide synthesizer (CEM SRL, Bergamo, Italy) by standard Fluorenylmethyloxycarbonyl strategy using H-Rink amide ChemMatrix resin (35–100 mesh particle size) as solid support on a 0.1 mmol scale. Peptide coupling was performed in dimethylformamide using the amino acid (4 equivalent), PyBOP (Benzotriazol-1-yloxy)

tripyrrolidinophosphonium hexafluorophosphate, 4 equivalent, and N,N-Diisopropylethylamine, 8 equivalents. The synthesis of T29-B also included additional conjugation with 8-amino 3,6-dioxaoctanoic acid linker at the terminal amino group to introduce a spacer between the targeting peptide and biotin. After the automatic synthesis, the resin-peptide (≈0.1 mmol of NH2 –terminated peptide) was mixed with a dimethylformamide solution of biotin-N-hydroxysuccinimide (0.3 mmol, 0.102 g) and N,N-Diisopropylethylamine (0.8 mmol, 0.143 mL). The mixture was stirred at room temperature for 12 hours, and the resin was thoroughly washed with dimethylformamide, dichloromethane, and diethylether. After cleavage and deprotection with trifluoroacetic acid (TFA) /Phenol/water/triisopropylsilane/ethanedithiol (82.5:5:5:5:2.5, v/v), the peptide was precipitated, and the solid was washed with diethyl ether. The solid was lyophilized to give the final product (68 mg, yield 36%, and purity 80% for T29-B and 60 mg, yield 33%, and purity 85% for F11-B). Analytical high-performance liquid chromatography-mass spectrometry (MS; Figure 1A, upper part for T29-B; and Figure 1B, upper part for F11-B) was performed on a Waters Fraction Lynx auto-purification system equipped with micromass ZQ ESI(+) ionization mode and dual-γ detectors, using Waters Atlantis RP-C18 column, 5 µm, 4.6 mm×150 mm and H_2O/0.1% TFA and CH_3CN/0.1% TFA as eluents. Method: initial condition 15% CH_3CN/0.1% TFA, linear gradient 15% to 30% CH_3CN/0.1% TFA over 12.5 minutes, 30% to 100% CH_3CN/0.1% TFA over 17.5 minutes, flow rate 1 mL/min, detection UV at 220 nm. T29-B: t_R= 18.4 minutes, ESI-MS (m/z); observed: 959.6 $[M+2H]^{2+}$, 1918.6 $[M+H]^+$ (Figure 1A, insert); calculated for $C_{82}H_{131}N_{19}O_{20}S$: 960.0, 1918.1. F11-B: t_R= 22.0 minutes, ESI-MS (m/z); observed: 600.3 $[M+3H]^{3+}$, 827.5 $[M+2H]^{2+}$, 1655 $[M+H]^+$ (Figure 1A, insert); calculated for $C_{76}H_{119}N_{17}O_{18}S_3$: 600.7, 900.6, and 1655. Absorbance at 280 nm of T29-B (Figure 1A, lower part) and F11-B (Figure 1B, lower part) was used to calculate their concentration, whereas their purification was performed by preparative high-performance liquid chromatography using a buffered solution of ammonium acetate as eluent.

TG Activity Assay

TG activity was determined as previously reported[22,23] using solid-phase microtiter plates coated with N,N′-dimethylcasein (20 mg/mL; overnight at 4°C). The unbound N,N′-dimethylcasein was discarded, and the wells were blocked with Tris [tris (hydroxymethyl)aminomethane)] 0.1 mmol/L, pH=8.5 supplemented with 3% bovine serum albumin (BSA). Before being added to the reaction, 10 µg FXIII (Enzyme Research Laboratories, South Bend, IN) was activated by incubation with 40 U/mL National Institutes of Health human thrombin for 45 minutes at room temperature. The cross-linking reactions of SAs were performed in a total volume of 200 µL containing 1 mmol/L of SAs, 0.1 mol/L $CaCl_2$, 0.1 mol/L Tris, 0.05 mol/L dithiothreitol, and gpTG2 13 µg (≥1.5 U/mg; Figure 1C) or FXIII (Figure 1D). Reactions were performed, while incubated at 37°C for 1 hour and were stopped by washing with 50 mmol/L ethylenediaminetetraacetic acid. The incorporated SAs were detected using 1:150 streptavidin-alkaline phosphatase with phosphatase substrate. Kinetic measurements of absorbance at 405 nm were determined at 15 seconds intervals for a period of 5 minutes (VICTOR2; Wallac, 1420 Multilabel counter; Winpact Scientific Inc, Irvine, CA). Relative activity of TG2 is expressed as units of absorbance. (*N*-(5-Aminopentyl)biotinamide (Cadaverine-B; BP; Pierce, Rockford, IL), nonspecific TG substrate, was used as a positive control. As negative control, the reaction mixture contained ethylenediaminetetraacetic acid (50 mmol/L) instead of $CaCl_2$. Measurements were analyzed as the ratio between the absorbance intensity of the reacted peptide to the absorbance intensity of the negative control. The values are mean±SD (n=3). **P*<0.05 versus F11-B and ***P*<0.05 versus T29-B.

Immunohistochemistry

Uterus sections containing hemizygote embryos of Myr-Venus on E5.5 (Figure 1A and 1E) or E6.5 Figure 2A and 2E) or surrogate Institute of Cancer Research (ICR) mice carrying embryos with transgenic TC on E6.5 (Figure 2 and 5) were fixed in 4% paraformaldehyde and later embedded in paraffin blocks and sectioned serially at a 4 µm thickness. The paraffin sections were deparaffinized with xylene for 15 minutes, followed by sequential ethanol hydration and double-distilled water. Sections were then washed with PBS followed by antigen retrieval in Citrate (pH 6.0) or ethylenediaminetetraacetic acid (pH 8.5) buffer using a pressure cooker at 125°C for 3 minutes. Thereafter, samples were blocked and permeabilized by 20% horse serum and 0.2% Triton X-100 in PBS. The following primary antibodies were added to the samples and incubated overnight at 4°C: mouse anti-TG2, mouse anti-FXIII (Abcam, Cambridge, United Kingdom) and goat anti-GFP (green fluorescent protein), rat anti-CD34 (cluster of differentiation 34; CEDARLANE, Burlington, NC), anti-CIV (collagen IV) antibody biotin conjugate (600-406-106, Rockland Immunochemicals Inc, Limerick, PA) and rabbit anti-fibrinogen (ab34269; Abcam, Cambridge, United Kingdom). Next, slides were washed with PBS and incubated with the appropriate secondary antibodies diluted 1:150 in PBS for 45 minutes at room temperature: CY5, Cy3, or Cy2-conjugated streptavidin, Cy3 anti-mouse (Jackson Immunoresearch Laboratories, West Grove, PA) or Alexa488 anti-goat. Please see the Major Resources Table in the online-only Data Supplement for additional information. Cell nuclei were fluorescently stained with DAPI. The fluorescent signal was detected in ×5, ×10, or ×20 magnifications using a fluorescent microscope (Zeiss Axioscope II, Yena, Germany, Simple PCI software). Images were processed as described earlier using ImageJ software.

Histological Analysis of TG2 and FXIII Activities

SAs T29 for TG2 and F11 for FXIII were synthetized based on a phage-displayed random peptide library screen.[24,26,28] Sections of mice uteri were used for histological mapping of TG2 and FXIII activities, according to the method described by Kawamoto[29,30] with slight modifications. Briefly, 8 to 12 weeks old C57bl/6J female mice (Envigo, Jerusalem, Israel) were mated with Myr-Venus[31] homozygote males to produce hemizygote embryos for Myr-Venus. On E5.5 or E6.5 the dams were injected IV with 0.1 mmol/L of T29-B or F11-B dissolved in PBS with 3% DMSO. Forty-five minutes after injection mice were euthanized, and their uteri were freeze-embedded with optimum cutting temperature compound (Tissue-Tek, Sakura Finetek, CA). Fifteen micrometer thick sections were prepared from the frozen specimen block using a cryomicrotome (Leica Co Ltd, Wetzlar, Germany).

Uteri sections of untreated C57bl/6J pregnant mice were used for detecting TG2 and FXIII activities by in situ

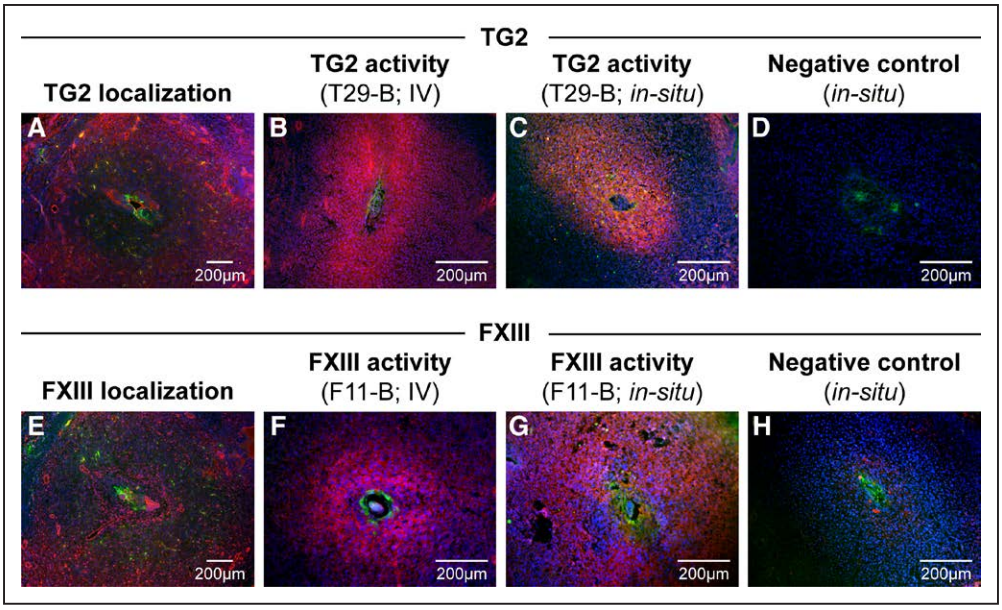

Figure 1. TG2 (tissue TG) and FXIII (factor XIII) activities, detected by (substrate analogs) SAs distribution, resemble their localization in implantation sites (ISs) retrieved from E5.5 pregnant C57bl/6J mice.
Myr-Venus homozygote males were mated with C57bl/6J female mice, producing hemizygote Myr-Venus embryos. **A**, TG2 localization in paraffin sections of embryo IS. Red represents antibody staining for TG2 (4 dams, 20 ISs). **B** and **C**, TG2 activity, detected by T29-B distribution 45 min after it was injected intravenously (**B**, 4 dams, 14 ISs) or applied in situ on live sections (**C**, 4 dams, 16 ISs). For images (**B** and **C**), red represents T29-B distribution, followed by Cy3-streptavidin staining. **D**, Negative control sections stained with Cy3-streptavidin staining without T29-B SA (5 dams, 20 ISs). **E**, FXIII distribution in paraffin sections of embryo IS (4 dams, 20 ISs). Red represents antibody staining for FXIII. **F** and **G**, FXIII activity, detected by F11-B distribution 45 min after it was injected intravenously (**F**, 5 dams, 17 ISs) or applied in situ on live sections (**G**, 4 dams, 11 ISs). For images (**F** and **G**), red represents F11-B distribution, following Cy3-streptavidine staining. **H**, Negative control sections stained with Cy3-streptavidin staining without F11-B SA (5 dams, 20 ISs). For all images: green represents hemizygote Myr-Venus embryos and blue DAPI staining. Image scale bars are 200 µm.

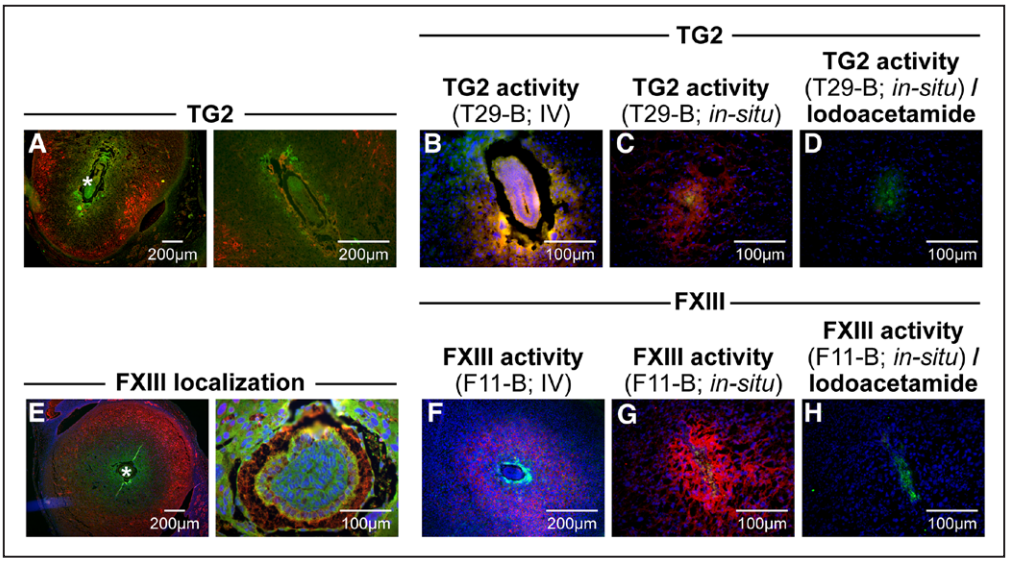

Figure 2. TG2 (tissue TG) and FXIII (factor XIII) specific activities matched their localization on the feto-maternal interface of implantation sites (ISs) retrieved from E6.5 pregnant C57bl/6J mice.
Myr-Venus homozygote males were mated with C57bl/6J female mice, producing hemizygote Myr-Venus embryos. **A**, **Left**, TG2 localization in paraffin sections of embryo IS. Red represent antibody for TG2. *Estimated embryonic region. **Right**, magnification of the marked region (3 dams, 24 ISs); TG2 activity, detected by T29-B distribution 45 min after it was injected intravenously (**B**, 3 dams, 13 ISs) or applied in situ on live sections (**C**, 4 dams, 18 ISs). **D**, TG2 specific activity, detected in situ on live sections after T29-B was applied in the presence of TG inhibitor, Iodoacetamide. For images (**B**–**D**), red represents T29-B distribution, following Cy3-streptavidin staining (4 dams, 16 ISs). **E**, **Left**, FXIII localization in paraffin sections of embryo IS. Red represents antibody for FXIII. *Estimated embryonic region. **Right**, magnification of the marked region (4 dams, 28 ISs); FXIII activity, detected by F11-B distribution 45 min after it was injected intravenously (**F**, 5 dams, 24 ISs) or applied in situ on live sections (**G**, 5 dams, 20 ISs). **H**, FXIII specific activity, detected in situ on live sections after F11-B was applied in the presence of Iodoacetamide (4 dams, 16 ISs). For images (**F**–**H**), red represents F11-B distribution, following Cy3-streptavidin staining. For all images: green represents hemizygote Myr-Venus embryos and DAPI in blue. Images scale bars are 100 or 200 µm.

administration of the SAs. Specificity of the SAs was also observed in situ by inhibiting TG activity with iodoacetamide. Sections were air dried and then blocked with 1% BSA at room temperature for 30 minutes. Sections were then incubated for 60 minutes at 37°C in the substrate reaction solution, consist of 100 mmol/L tris(hydroxymethyl)aminomethane (Tris; pH 8.0), 1 mmol/L dithiothreitol 5 mmol/L $CaCl_2$, and T29-B or F11-B at the final concentration of 10 µmol/L. Nonspecific activity of the SAs was detected by adding 1 mg/mL of iodoacetamide to the reaction solution. Enzymatic reaction was stopped using 50 mmol/L ethylenediaminetetraacetic acid. After fixation, all sections were blocked and incubated with Cy3-streptavidin (Jackson Immunoresearch Laboratories, West Grove, PA). IS with Myr-Venus hemizygote embryos were further treated with 1:500 goat anti-GFP (Abcam, Cambridge, United Kingdom) diluted in 20% horse serum and 0.2% Triton X-100 overnight at 4°C. Sections were treated with Alexa488 anti-goat (Abcam, Cambridge, United Kingdom) and cell nuclei and later stained by DAPI. Samples were observed under a fluorescence microscope using ×10 or ×20 magnifications (Zeiss Axioscope II, Yena, Germany, Simple PCI software). Vessel density was determined with Fluorescence images of anti-CD34 staining[10] using ImageJ software (Wayne Rasband, National Institutes of Health, MD). In brief, under identical conditions the fluorescence intensity of the stained area from the total IS area was measured in absolute counts after applying an automatic threshold. Fluorescent intensity outside the vessel area was masked and excluded from calculation. The average fluorescence intensity inside the IS region was calculated by measuring the ratio of fluorescence signal intensity to the area of region of interest.

Lentiviral Vectors Design and Production

Lentiviral vectors were constructed to induce expression of mouse TG2 or mouse FXIII (see Table I in the online-only Data Supplement for gene identifiers of TG2 and FXIII). Mouse TG2 and mouse FXIII were isolated from uterine cDNA restriction-free cloning using primers containing complementary overhangs to the designated target vector LV-GFP (Table II in the online-only Data Supplement). The purified PCR products were cloned into the lentiviral expression vector, LV-GFP (provided by Dr Oded Singer, Weizmann Institute of Science, Israel). To efficiently knockout of TG2 or FXIII, 2 single guide RNA (sgRNA) targeting TG2 or FXIII were used (Table II in the online-only Data Supplement). The guides were chosen to maximize on target scores and minimize off-target scores using several CRISPR designing tools, including the MIT CRISPR design tool[32] and sgRNA Designer, Rule Sets 1 and 2,[33,34] in both the original sites and in the Benchling implementations websites (www.benchling.com), SSC (sequence scan for CRISPR),[35] and sgRNA scorer.[36] The sgRNA guide sequences were cloned into lentiCRISPR v2 lentiviral vector (Dr Igor Ulitsky and Dr Yoav Lubelsky, Weizmann Institute, Israel) according to Sanjana et al[37] with slight modifications. Briefly, oligonucleotides for the TG2 or FXIII sgRNA guide sequences were phosphorylated using T4 PNK (NEB, Ipswich, MA) for 30 minutes at 37°C, then annealed by heating to 95°C for 5 minutes and cooled down to 25°C at 5°C/min. The lentiCRISPR v2 vector and the annealed oligos were then supplemented with FastDigest BsmBI (Thermo Fisher Fermentas, Waltham, MA) and T7 ligase (NEB, Ipswich, MA) by 6 cycles of 5 minutes at 37°C followed by 5 minutes at 23°C. The ligation reaction was next treated with PlasmidSafe exonuclease (NEB, Ipswich, MA) for 30 minutes at 37°C. Recombinant lentiviruses were produced by transient transfection[38] in HEK293FT cells (Invitrogen, Carlsbad, CA) using 3 envelope and packaging plasmids and one of the following viral construct: TG2-LV-GFP (TG2 overexpression), TG2-CRISPR-v2 (TG2 depletion), FXIII-LV-GFP (FXIII overexpression), FXIII-CRISPR-v2 (FXIII depletion), Control-LV-GFP (LV-GFP vector without insert), or Control-CRISPR-v2 (lentiCRISPR v2 vector without insert). Viral supernatants were harvested 48-hour post-transfection and filtered through a 0.45 µm pore cellulose acetate filters and concentrated by ultracentrifugation. Lentiviral supernatant titers were determined by Lenti-X p24 Rapid Titer Kit (Table II in the online-only Data Supplement) according to manufacturer's protocol (Takara Bio USA, Inc, CA).

TG2 and FXIII Overexpression Validation

Validation was conducted using Western Blot analysis (Figure 2D). HEK293FT cells at 90% confluence were seeded in a 6 well plate. The next day cells were infected by the constructed lentivirus: TG2-LV-GFP, FXIII-LV-GFP, or Control-LV-GFP. The following day cells were harvested, and 50 µg of cell lysates were separated by 12% polyacrylamide SDS-PAGE. Protein fractions were transferred on ice to nitrocellulose membranes (100 V for 1 hour; Whatman, Dassel, Germany). Membranes were blocked by incubation with 20 % BSA and 0.1% Tween-20 in Tris buffered for 2 hours at room temperature. Western blot analysis was performed by incubating first with primary mouse monoclonal anti-TG2 or anti-FXIII antibodies (1:500; Abcam, Cambridge, United Kingdom), followed by secondary anti-mouse horseradish peroxidase conjugate (Jackson ImmunoResearch, West Grove, PA) and visualized with ECL (Pierce, Rockford, IL). In addition, blastocysts from all 3 groups were stained by whole-mount incubation with antibodies against TG2 (Figure 2C) and FXIII (Figure 2D), stained with specie specific secondary antibodies, Cy3 anti-mouse (1:1000; Jackson Immunoresearch Laboratories, West Grove, PA), counterstained with 4′,6-diamidino-2-phenylindole (DAPI; 1:1000; Vector Laboratories, Burlingame, CA), subsequently mounted in mineral oil. Images were taken using spinning disk 386 confocal microscope using ×40 magnification (Zeiss, Cell observer SD, Yena, Germany).

Generation of Surrogate Mice Carrying Embryos With Genetically Modified TC

All animal experiments were approved by the Animal Care and Use Committee of the Weizmann Institute (Approval numbers: 20510915-2 and 26130416-1). Follicle development was induced by pregnant mare's serum gonadotropin (5 IU sc; PMSG; Sigma-Aldrich, Rehovot, Israel) in 21 days old wild-type ICR female mice (Harlan, Jerusalem, Israel). After 48 hours, ovulation was induced by human chorionic gonadotropin (5 IU SC; hCG; Sigma-Aldrich, Rehovot, Israel). PMSG/hCG-treated female mice were housed overnight with wild-type ICR males, and the next morning the presence of a vaginal plug was examined (defined as embryonic day 0.5; E0.5). The female mice were euthanized 3 days later, and embryos at the

morula or blastocyst stage were flushed out of the uteri. The embryos were incubated in potassium-supplemented simplex optimized medium to expand the blastocysts, and their Zona pellucida was removed in acidic Tyrode's solution.[39] Next, 20 to 40 embryos were incubated with lentiviruses in potassium-supplemented simplex optimized medium for 6 hours at 37°C and subsequently were washed 4 times.[6] Before embryo transfer blastocysts (Figure 2A) expressing control vector or overexpressing TG2 or FXIII were visualized for GFP expression. Using Nonsurgical embryo transfer kit (NSET, ParaTechs, Lexington, KY), 10 blastocysts were transplanted into E2.5 pseudopregnant ICR female mouse. Pseudopregnancy was achieved by mating the wild-type ICR females with vasectomized males of proven sterility.

DCE-MRI Studies

DCE-MRI experiments were performed on a horizontal bore 9.4 T Biospec spectrometer using a linear coil for excitation and detection (Bruker BioSpin GmbH, Ettlingen, Germany), as previously reported.[10,40,41] Surrogate E6.5 pregnant mice carrying genetically modified embryos were serially scanned (each group consisted of 3–5 dams with 1–3 ISs). Mice were kept under respiratory monitoring while anesthetized by isoflurane (Abbott Laboratories, North Chicago, IL). The BSA-based macromolecular contrast material (biotin-BSA-GdDTPA [gadolinium diethylenetriaminepentaacetic acid]; 80 kDa; r=164 mmol/L^{-1} s^{-1}; Symo-Chem, Eindhoven, the Netherlands), was administered via a tail vein catheter as bolus at 10 mg/mouse in 0.2 mL of PBS. Series of variable-flip-angle precontrast T1-weighted 3D gradient-echo images of the IS were acquired, before and sequentially 40 minutes after injecting the contrast agent. Variable-flip-angle precontrast T_1-weighted 3D-gradient-echo images were acquired to determine the precontrast R_1 (repetition time: 10 ms; echo time: 2.8 ms; flip angles: 5°, 15°, 30°, 50°, and 70°; 2 averages; matrix: 256×256×64; field of view: 35×35×35 mm^3). The post-contrast images were obtained with a single flip angle (15°). Hyper permeable blood vessels were examined 40 minutes after biotin-BSA-GdDTPA injection (Figure 3G through 3I, left side). Functional blood vessels were also confirmed in histological sections after intravenous injection of BSA labeled with 6-carboxy-X-rhodamine (BSA-ROX; 10 mg/mouse in 0.2 mL of PBS), 2 minutes before euthanizing the mice (Figure 3G through 3I, right side). BSA was labeled with rhodamine 5(6)-carboxy-X-rhodamine succinimidyl ester (BSA-ROX; Molecular Probes, Eugene, OR) as reported previously,[42] producing a labeling ranged between 2 to 4 fluorophores per protein molecule. Change in contrast agent concentration in the region of interest over time (C_t) was divided by its blood concentration (C_{blood}; extrapolated from vena cava region as time 0). Linear regression of these temporal changes in C_t/C_{blood} yielded 2 vascular parameters: Fractional blood volume (fBV=C_0/C_{blood}) describes blood vessel density and is derived from the extrapolated concentration of the contrast agent in the IS at time zero, divided by the measured concentration in the vena cava, ≈5 minutes after intravenous administration. Permeability surface area product (PS=[C_t−C_0]/[C_{blood}×t]) depicting rate of contrast agent extravasation from blood vessels and its accumulation in the interstitial space, was derived from the slope of the linear regression of the first 15 minutes after contrast material administration (t=15). Mean fractional blood volume and PS were calculated separately for single IS.

Statistical Analysis

All experiments were repeated at least 3× using GraphPad Prism software version 8.0.0 for Windows (GraphPad Software, San Diego, CA, www.graphpad.com). Statistically significant differences between experimental groups were analyzed with nonparametric post hoc test (Tukey-Kramer), as it was not normally distributed according to the Shapiro-Wilk test. The number of dams and ISs of each experiment indicated accordingly. Data are presented as mean±SD with P values <0.05 considered significant.

RESULTS

TG Expression and Enzymatic Activity in Embryo ISs

ISs at E5.5 (Figure 1) and E6.5 (Figure 2) were characterized for the localization and activity of TG2 and FXIII. At E5.5, TG2 was detected in TC (Figure 1A) while FXIII was detected within the implantation chamber (Figure 1E). TG2 and FXIII activity in vivo was assessed on frozen sections derived from IS after intravenous injection of T29-B (Figure 1B) or F11-B (Figure 1F) to E5.5 pregnant mice. Total TG2 and FXIII activities was detected in situ by exposing fresh sections of nontreated IS to T29-B (Figure 1C) or F11-B (Figure 1G). Negative controls for T29-B (Figure 1D) or F11-B (Figure 1H) showed inconsiderable signals on in situ labeling with secondary antibodies without the SAs presence. On IS retrieved from E6.5 pregnant mice, TG2 (Figure 2A) or FXIII (Figure 2E) were further detected on the secondary decidual zone contra-position the mesometrial side. Similar distribution pattern of T29-B (Figure 2A and 2C) or F11-B (Figure 2F and 2G) on E6.5 IS was detected, after both intravenously in vivo and in situ administration of the SA. Nonspecific incorporation of T29-B (Figure 2D) or F11-B (Figure 2H) was negligible as demonstrated in situ using the TG inhibitor iodoacetamide. Comparison of IS on E5.5 and E6.5 revealed substantial changes in TG2 and FXIII localizations. While on E5.5, TG2 and FXIII were mainly localized around the embryo, their expression shifted toward the mesometrial side, concentrating at the IS boundaries. Interestingly, FXIII localization in IS on E5.5 was associated within cell nuclear surrounding the embryo. This unexpected association was not detected on E6.5.

MRI Reveals a Role for TG2 and FXIII in Maternal Angiogenesis During Embryo Implantation

The role of TG2 and FXIII with decidual vascular remodeling was examined by DCE-MRI of E6.5 surrogate pregnant mice carrying embryos with transgenic troph-

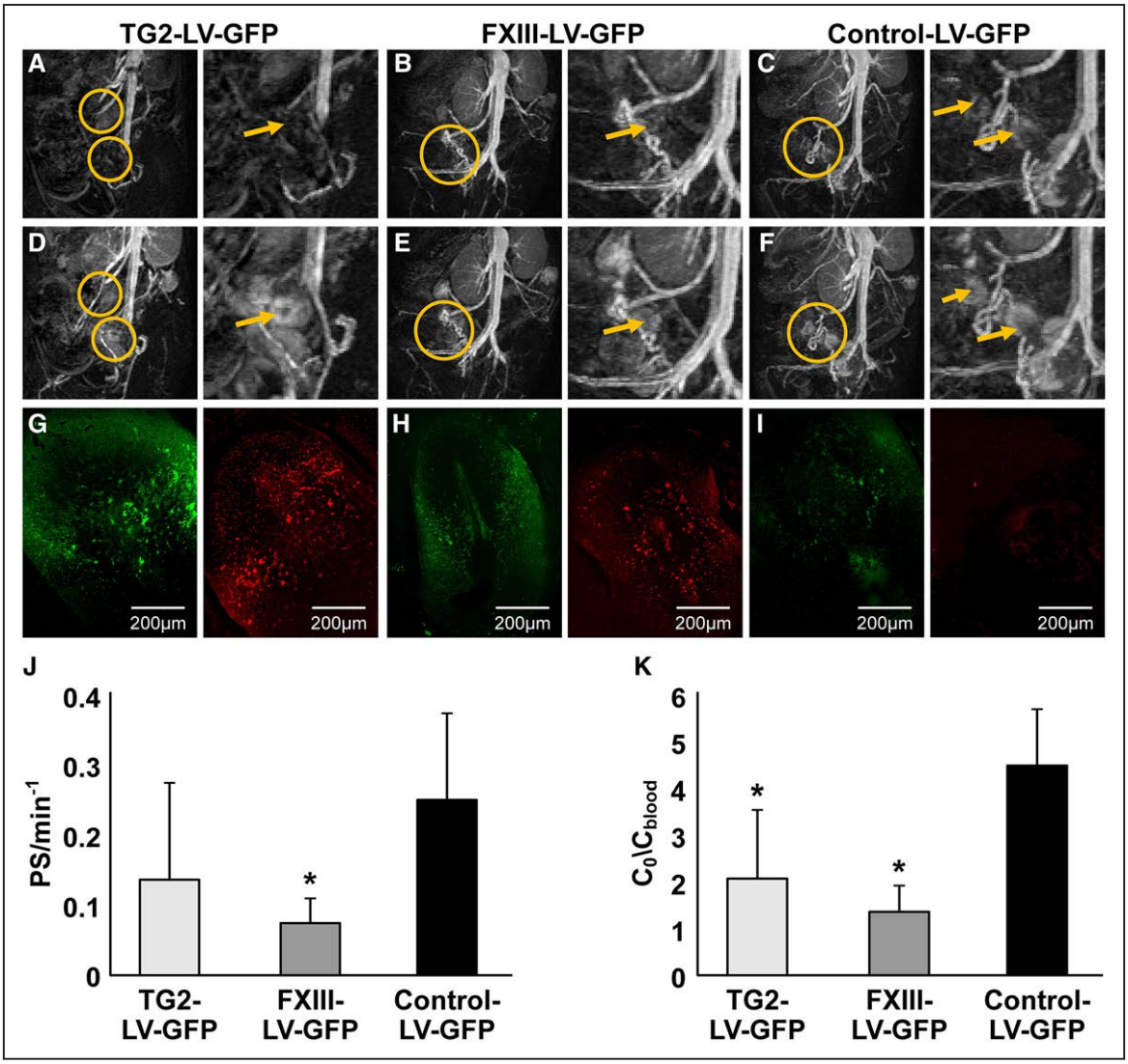

Figure 3. Impaired decidual vascular function of (implantation sites) ISs with genetically modified trophoblast cells (TC) overexpressing TG2 (tissue TG) or FXIII (factor XIII).

T1-weighted gradient-echo images acquired from surrogate E6.5 pregnant ICR (Institute of Cancer Research) mice carrying transgenic embryonic TC overexpressing TG2 (**A** and **D**; TG2-LV-GFP [lentivirus vector-green fluorescent protein]), overexpressing FXIII (**B** and **E**; FXIII-LV-GFP) or expressing the control vector (**C** and **F**; Control-LV-GFP), 3 min (**A**–**C**) or 40 min (**D**–**F**) after biotin-BSA-GdDTPA (gadolinium diethylenetriaminepentaacetic acid) injection. Individual ISs are indicated by orange circles. **Right**, magnification of the adjacent **left** image; Validation of the decidual blood vessels permeability functions by visualizing biotin-BSA-GdDTPA distribution in paraffin sections of ISs with transgenic embryonic TC overexpressing TG2 (**G**, **Left**), overexpressing FXIII (**H**, **Left**) or expressing the control vector (**I**, **Left**). Green represent contrast agent distribution, 40 min after it was injected, using streptavidin-Cy2 staining; Validation of functional decidual blood vessels by detecting BSA-ROX (bovine serum albumin-6-carboxy-X-rhodamine) distribution in paraffin sections of ISs with transgenic embryonic TC overexpressing TG2 (**G**, **Right**), overexpressing FXIII (**H**, **Right**) or expressing the control vector (**I**, **Right**). Red represents the distribution of BSA-ROX, 2 min after it was injected; Quantitative analysis of vessel density and vascular permeability in the ISs using the magnetic resonance imaging parameters: permeability surface area product (**J**) and fraction blood volume (**K**). The values are calculated as mean±SD of transgenic embryos overexpressing TG2 (4 dams, 12 ISs), overexpressing FXIII (5 dams, 19 ISs) or expressing the control vector (5 dams, 13 ISs). **P*<0.05 vs Control-LV-GFP. Image scale bars are 200 μm.

ectoderm induced by lentiviral infection of blastocysts. Significantly low PS (Figure 3J) values, consistent with attenuated extravasation of the MRI contrast agent, were measured in the IS with TC overexpressing FXIII (Figure 3B and 3E) but not overexpressing TG2 (Figure 3A and 3D) relative to the control group (Figure 3C and 3F). Fractional blood volume (Figure 3K) was reduced significantly at IS of embryos with TC overexpressing either FXIII or TG2. Accordingly, decreased histological labeling of biotin-BSA-GdDTPA was observed in IS with overexpressing TG2-(Figure 3G, left) or FXIII-(Figure 3H, left) TC, compared with IS with control vector (3I, left). As opposed to IS sections with TC overexpressing TG2 (Figure 3G, right) or those expressing the control vector (Figure 3I, right), fluorescent BSA (BSA-ROX) was hardly detected in is with FXIII-overexpressing TC (Fig-

ure 3H, right). PS values (Figure 4J) calculated from IS in which either TG2 (Figure 4A and 4D) or FXIII (Figure 4B and 4E) were depleted from TC using lentiCRISPR v2 lentiviral vector were not significantly different from the control (Figure 4C and 4F). A significant increase in PS values was measured from IS with FXIII-depleted TC (Figure 4K) relative to the control IS and also to the values calculated from IS with TG2-depleted TC. While IS with TG2-depleted TC (Figure 4K) revealed no significant changes compared with the control values. Histological cross sections of these IS were used to corroborate the changes in blood volume and perme-

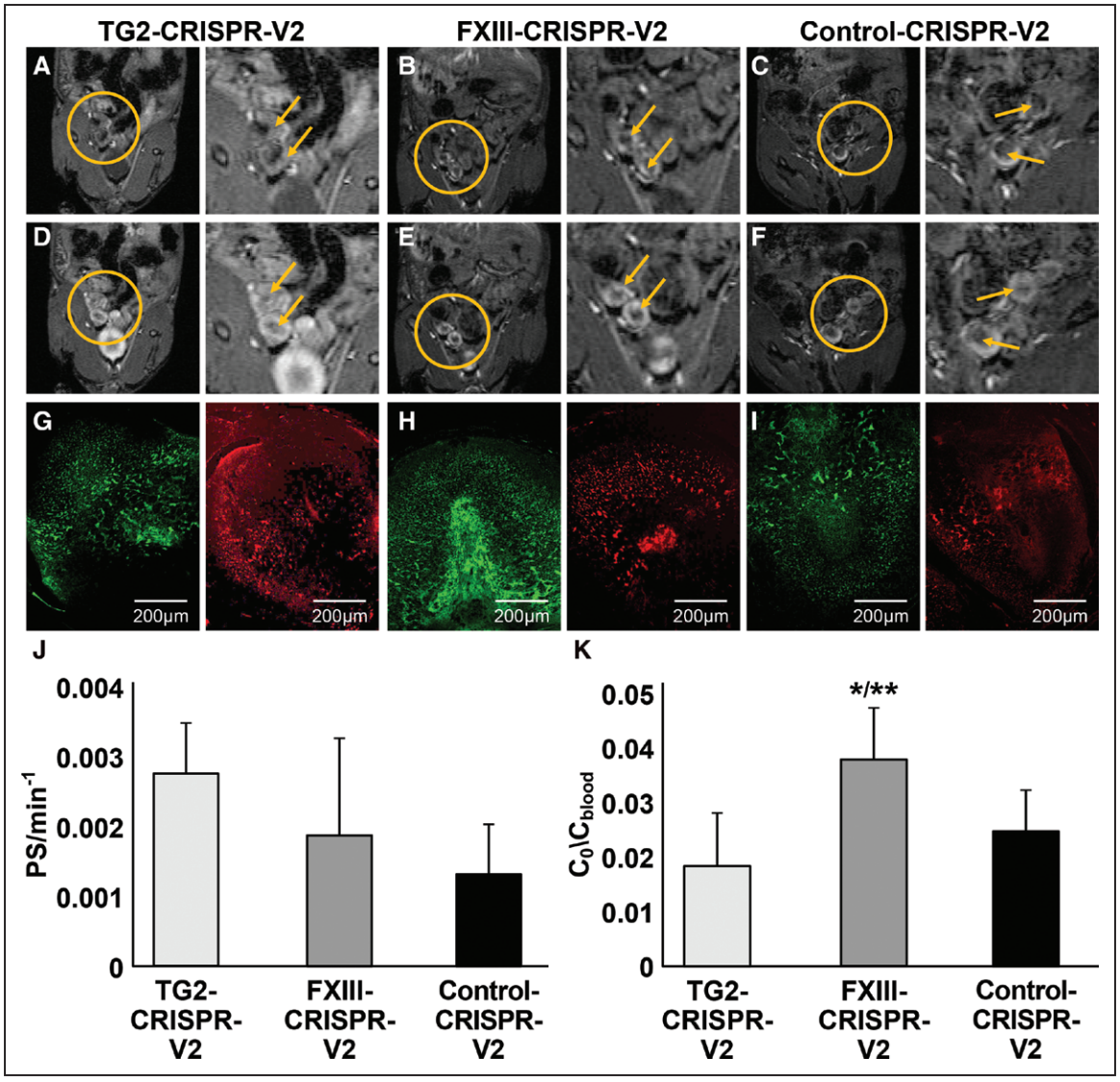

Figure 4. Decidual blood vessel function increased in (implantation sites) ISs with TG2 (tissue TG)-or FXIII (factor XIII)-depleted embryonic TC (transglutaminase).
T1-weighted gradient-echo images acquired from surrogate pregnant ICR (Institute of Cancer Research) mice carrying embryos with genetically modified TC depleted from TG2 (**A** and **D**; TG2-CRISPR [clustered regularly interspaced short palindromic repeats]-V2), depleted from FXIII (**B** and **E**; FXIII-CRISPR-V2) or expressing the control vector (**C** and **F**; Control-CRISPR-V2), 3 min (**A**–**C**) or 40 min (**D**–**F**) after biotin-BSA-GdDTPA (gadolinium diethylenetriaminepentaacetic acid) injection. Individual ISs are indicated by orange circles. **Right** side, magnification of the adjacent **left** image; Validation of the decidual blood vessels permeability by visualizing biotin-BSA-GdDTPA distribution in paraffin sections of ISs with embryonic TC depleted from TG2 (**D**, **Left**; TG2-CRISPR-V2), depleted from FXIII (**E**, **Left**; FXIII-CRISPR-V2) or expressing the control vector (**F**, **Left**; Control-CRISPR-V2), Green represent the distribution of the contrast agent 40 min after injection using streptavidin-Cy2 staining. Validation of functional decidual blood vessels by detecting BSA-ROX (bovine serum albumin-6-carboxy-X-rhodamine) distribution in paraffin sections of ISs with embryonic TC depleted from TG2 (**G**, **Right**; TG2-CRISPR-V2), depleted from FXIII (**H**, **Right**; FXIII-CRISPR-V2) or expressing the control vector (**I**, **Right**; Control-CRISPR-V2), Red represents the distribution of BSA-ROX injected 2 min before euthanizing the mouse. Quantitative analysis using the magnetic resonance imaging parameters: permeability surface area product (**J**) and fraction blood volume (**K**). The values are calculated as mean±SD of transgenic embryo models depleted from TG2 (3 dams, 10 ISs), FXIII (4 dams, 12 ISs), or expressing the control vector (4 dams, 9 ISs), PS: *P<0.05 vs Control-CRISPR-V2; **P<0.05 vs TG2-CRISPR-V2. Images scale bars are 200 μm.

ability detected by the MRI. In IS with TG2-depleted TC (Figure 4G, left), biotin-BSA-GdDTPA was mainly distributed in the secondary decidual zone. Slight reduction in BSA-ROX distribution was observed in IS with TG2-depleted TC (Figure 4G, right) as compared with the control group (Figure 4I, right). Interestingly, the contrast agent was clearly detected in the embryonic niche of IS with FXIII-depleted TC (Figure 4H). IS vasculature was further characterized by CD34 (cluster of differentiation 34) staining for angiogenic neovasculature (Figure 5). CD34 in control IS (Figure 5A, 5C, 5E, and 5G) was distributed in a mesh-like pattern, arrayed intensely on the anti-mesometrial region. Vessels expressing CD34 were detected in IS with TC overexpressing TG2 (Figure 5B) or TG2-depleted TC (Figure 5D). The organized vascular structure visualized by CD34 labeling of the control IS (Figure 5E), could not be detected on IS with TC overexpressing FXIII (Figure 5F). CD34 staining was elevated in IS with FXIII-depleted TC (Figure 5H) relative to control (Figure 5G). Quantitative analysis of the detected CD34 signal intensity, showed no significant difference between IS with TC overexpressing TG2 (Figure 5I) or TG2-depleted TC (Figure 5J) compared with control sections. However, IS with TC overexpressing FXIII (Figure 5K) demonstrated a significant lower signal intensity while, IS with FXIII-depleted TC (Figure 5K) had significant higher signal intensity than their control.

Fibrinogen and Collagen Intravenously Remodeling Is Mediated by FXIII During Implantation

Fibrinogen was clearly detected in the anti-mesometrial pole and adjacent to control embryonic TC (Figure 5A, upper part). Increased fibrinogen deposition was detected in IS of FXIII-overexpressing TC, particularly in

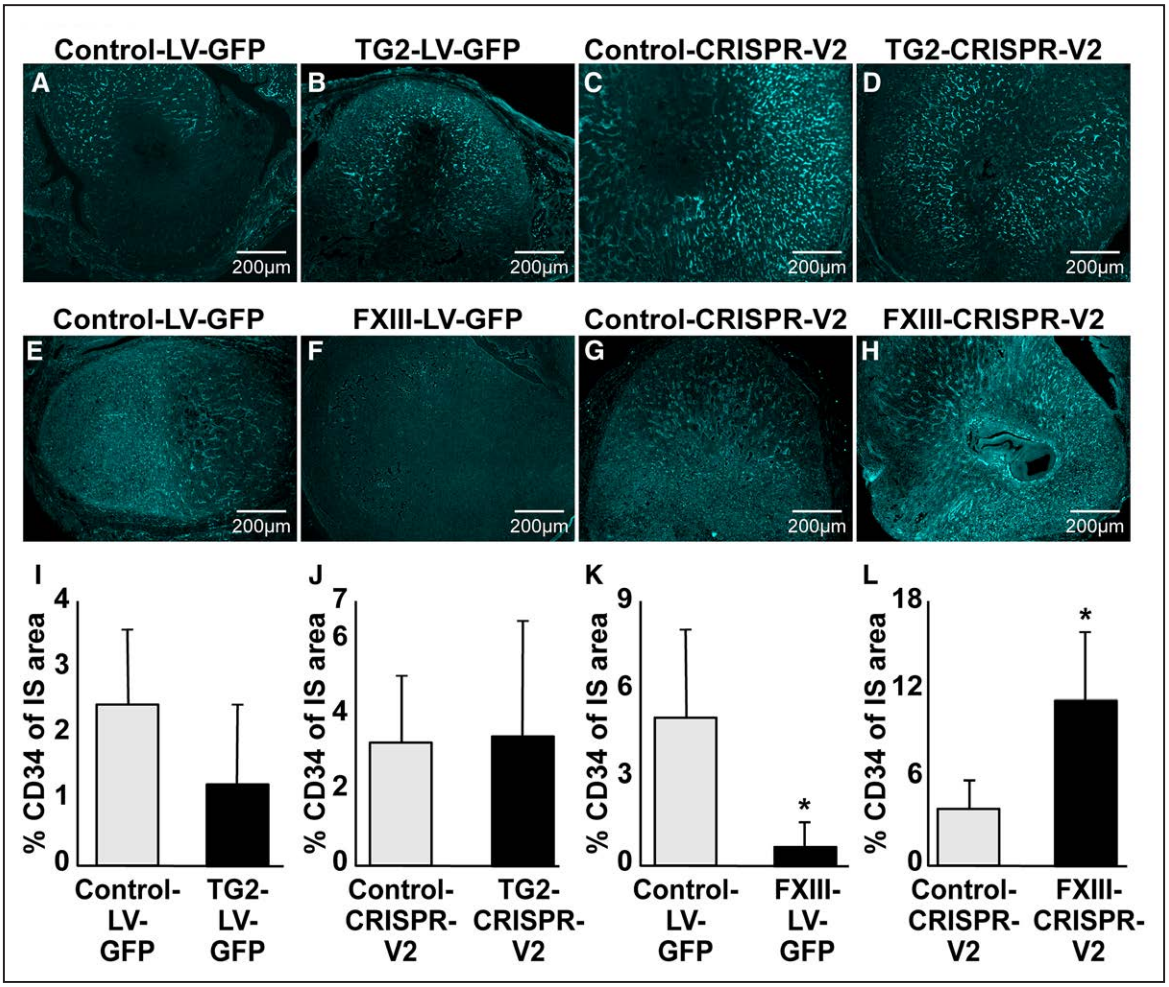

Figure 5. Microvascular evaluation of the implantation site (ISs) with transgenic embryos.
Immunostaining for CD34 (cluster of differentiation 34) in ISs of genetically modified TC expressing the control vector (LV-GFP [lentivirus-green fluorescent protein], **A** and **E**; CRISPR-V2, **C** and **G**, both 4 dams, 10 ISs), overexpressing TG2 (TG2-LV-GFP; **B**, 4 dams, 12 ISs), depleted from TG2 (tissue TG; **D**, 3 dams, 10 ISs), overexpressing FXIII (factor XIII; **F**, 5 dams, 19 ISs) or depleted from FXIII (**H**, 4 dams, 12 ISs). CD34 was visualized by cyan fluorescence channel after labeled with Cy5-avidin. Similar exposure time was used for each section and its appropriate control. Quantitative analysis of % CD34 staining in relation to IS area of genetically modified TC overexpressing TG2 (**I**), depleted from TG2 (**J**), overexpressing FXIII (**K**) or depleted from FXIII (**L**). Image scale bars are 200 μm. **P*<0.05 vs control vector.

the IS circumference, while fibrinogen was diminished at the embryonic vicinity (Figure 5B, upper part), as compared with control. CIV localization on the control IS (Figure 5A, lower part) was confined to the anti-mesometrial pole and around the primary decidual zone, while a substantial wider partition was displayed on the FXIII overexpressed TC (Figure 5B, lower part). Inversely to the IS with FXIII overexpressed TC, fibrinogen and CIV were hardly detected in IS with FXIII-depleted TC (Figure 5D) relative to control (Figure 5C).

DISCUSSION

In this study, MRI was applied for detection of the role of the 2 TG isoenzymes, TG2 and FXIII, in decidual angiogenesis during early embryo implantation (Figure 6). TG2 and FXIII were expressed mostly at the feto-maternal interface and at the decidual anti-mesometrial pole at E5.5. and E6.5. Association between FXIII localization to cell nuclei was observed in the IS. Beyond the role of secreted FXIII in coagulation, it also mediates intranuclear cross-linking.[43] The role of TG isoenzymes on implantation was determined by manipulating TG2 and FXIII expression in embryonic TC. DCE-MRI showed reduced decidual vascular density in IS with TC overexpressing TG2, and elevated permeability in IS with TG2-depleted TC (Figure 6B). Decidual vasculature did not show significant changes when TG2 was depleted from TC. DCE-MRI revealed that TC derived FXIII regulates decidual vascular density. Substantially, low fractional blood volume as well as low PS values were detected in IS where the TC overexpressed FXIII. IS with FXIII-depleted TC showed increased transcapillary leakage with higher PS values (Figure 6C) than IS of embryonic TC infected with an empty control vector (Figure 6A). Embryo implantation failure is the primary cause for the low success of in vitro fertilization programs.[4] Impaired uterine hyperpermeability has been widely proposed as an important cause for implantation failure in humans.[44] Several complications of pregnancy, such as preeclampsia and intrauterine growth restriction, have been attributed to disturbances in early uterine blood supply[12] or impaired trophoblast invasion of the placental bed spiral arterioles later in pregnancy.[13] Therefore, it is important to characterize the processes regulating uterine extracellular-matrix remodeling and angiogenesis during implantation, and MRI (specifically DCE-MRI) is a powerful tool addressing research requirements.

In our study, fibrinogen appeared to be diminished at the feto-maternal interface of the FXIII overexpressed IS, while it was increased on the decidua circumference. On the contrary, CIV was highly detected in IS with FXIII overexpressed TC extending further into the decidua, while it was narrowly confined around the control's embryo. Both fibrinogen and CIV were hardly detected in the IS with FXIII-depleted TC. Our findings indicate that enhanced activity of FXIII is associated with CIV presence. The precise role of FXIII in changing the fibrinogen distribution pattern is unclear. It is possible that FXIII and CIV take part in anchoring the embryo to the endometrium as suggested by Asahina.[45]

Association between abnormal expression levels of TG2 or FXIII (CD) to both reduced fertility and increased risk of adverse pregnancy-related events has been long documented.[46,47] The activities of TG2 and FXIII were evaluated here using novel selective substrate analogs, T29-B and F11-B, respectively, suggesting their potential as molecular imaging probes in selective detection

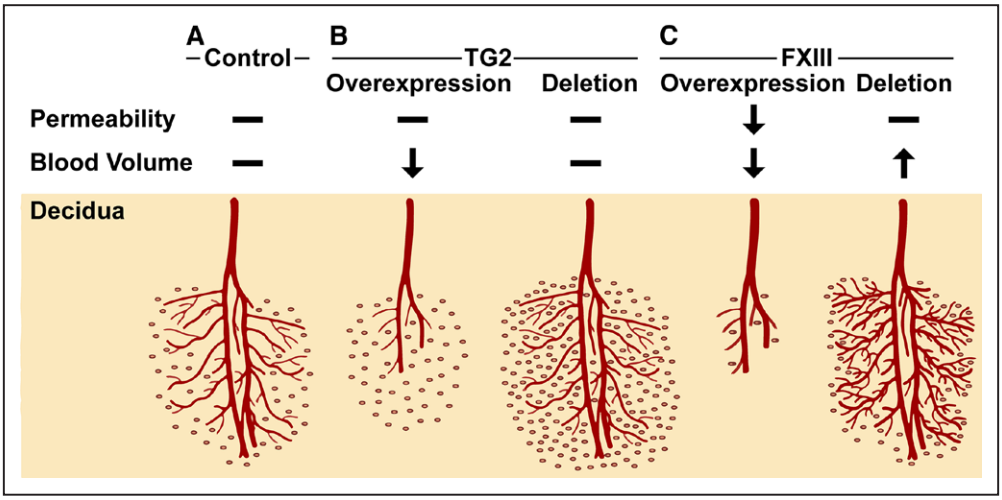

Figure 6. The effect of trophoblast cell (TC) derived TG2 (tissue TG) or FXIII (factor XIII) on the decidual vascular function. **A**, Decidual blood vessels permeability and blood volume; Embryo TC infected by lentivirus to overexpressing TG2 (**B**, **Left**) or FXIII (**C**, **Left**), display a decrease in decidual blood volume. Overexpressing of FXIII also shows a significant decrease in decidual blood vessels permeability (**C**, **Left**); Decidual vasculature properties did not change when embryonic TC was depleted of TG2 (**B**, **Right**), while depletion of FXIII (**C**, **Right**) shows a significant increase in decidual blood volume. Red branched lines represent blood vessels density; ovals represent blood vessel permeability.

of TG2 and FXIII. TG isoenzyme localization showed a direct correlation to their SA distribution. Establishment of implantation sites with genetically modified TC, enabled us to study the effect on maternal angiogenesis on TG2 and FXIII modulation. Our findings demonstrated that TC derived TG2 plays an important role in regulating decidual vascular permeability, while TC derived FXIII regulates vascular density as well as permeability. These findings suggest distinct roles for TG2 and FXIII during embryo implantation and may shed light on TG-reduced fertility. Moreover, MRI provides a modality of choice for high resolution in vivo imaging of the early stages of pregnancy, and particularly the maternal angiogenesis induced by the implanting embryo.

ARTICLE INFORMATION

Received on: December 19, 2018; final version accepted on: May 10, 2019.

Affiliations

From the Department of Biological Regulation (G.C., R.H., F.K., N.D., M.N.) and Life Science Core Facilities (S.B.-D.), Weizmann Institute of Science, Rehovot, Israel; Department of Molecular Biotechnology and Health Sciences, University of Torino, Italy (R.S., A.P., D.L., S.A.); and Department of Ruminant Science, Agricultural Research Organization, Bet Dagan, Israel (M.E., E.G.).

Acknowledgments

M. Neeman is incumbent of the Helen and Morris Mauerberger Chair in Biological Sciences. G. Cohen, R. Hadas, R. Stefania, A. Pagoto, D. Longo, and M. Elbaz performed experiments and analyzed data. S. Ben-Dor analyzed data. F. Kohen assisted in protocol design. G. Cohen, R. Hadas, N. Dekel, E. Gershon, S. Aime, and M. Neeman designed the study and wrote the article.

Sources of Funding

This work was supported by the Seventh Framework European Research Council Advanced Grant 232640-IMAGO and by National Institutes of Health (grant 1R01HD086323).

Disclosures

None.

REFERENCES

1. Zhang S, Lin H, Kong S, Wang S, Wang H, Wang H, Armant DR. Physiological and molecular determinants of embryo implantation. *Mol Aspects Med*. 2013;34:939–980. doi: 10.1016/j.mam.2012.12.011
2. Dey SK, Lim H, Das SK, Reese J, Paria BC, Daikoku T, Wang H. Molecular cues to implantation. *Endocr Rev*. 2004;25:341–373. doi: 10.1210/er.2003-0020
3. Welsh AO, Enders AC. Chorioallantoic placenta formation in the rat: II. Angiogenesis and maternal blood circulation in the mesometrial region of the implantation chamber prior to placenta formation. *Am J Anat*. 1991;192:347–365. doi: 10.1002/aja.1001920404
4. Cha J, Sun X, Dey SK. Mechanisms of implantation: strategies for successful pregnancy. *Nat Med*. 2012;18:1754–1767. doi: 10.1038/nm.3012
5. Sharkey AM, Smith SK. The endometrium as a cause of implantation failure. *Best Pract Res Clin Obstet Gynaecol*. 2003;17:289–307.
6. Georgiades P, Cox B, Gertsenstein M, Chawengsaksophak K, Rossant J. Trophoblast-specific gene manipulation using lentivirus-based vectors. *Biotechniques*. 2007;42:317–318, 320, 322. doi: 10.2144/000112341
7. Carson DD, Bagchi I, Dey SK, Enders AC, Fazleabas AT, Lessey BA, Yoshinaga K. Embryo implantation. *Dev Biol*. 2000;223:217–237. doi: 10.1006/dbio.2000.9767
8. Matsumoto H, Ma WG, Daikoku T, Zhao X, Paria BC, Das SK, Trzaskos JM, Dey SK. Cyclooxygenase-2 differentially directs uterine angiogenesis during implantation in mice. *J Biol Chem*. 2002;277:29260–29267. doi: 10.1074/jbc.M203996200
9. Plaisier M. Decidualisation and angiogenesis. *Best Pract Res Clin Obstet Gynaecol*. 2011;25:259–271. doi: 10.1016/j.bpobgyn.2010.10.011
10. Plaks V, Birnberg T, Berkutzki T, Sela S, BenYashar A, Kalchenko V, Mor G, Keshet E, Dekel N, Neeman M, Jung S. Uterine DCs are crucial for decidua formation during embryo implantation in mice. *J Clin Invest*. 2008;118:3954–3965. doi: 10.1172/JCI36682
11. Quenby S, Farquharson RG, Dawood F, Hughes AM, Topping J. Recurrent miscarriage and long-term thrombosis risk: a case-control study. *Hum Reprod*. 2005;20:1729–1732. doi: 10.1093/humrep/deh844
12. Redman CW, Sargent IL. Latest advances in understanding preeclampsia. *Science*. 2005;308:1592–1594. doi: 10.1126/science.1111726
13. Hanna J, Goldman-Wohl D, Hamani Y, et al. Decidual NK cells regulate key developmental processes at the human fetal-maternal interface. *Nat Med*. 2006;12:1065–1074. doi: 10.1038/nm1452
14. Eckert RL, Kaartinen MT, Nurminskaya M, Belkin AM, Colak G, Johnson GV, Mehta K. Transglutaminase regulation of cell function. *Physiol Rev*. 2014;94:383–417. doi: 10.1152/physrev.00019.2013
15. Wang Z, Perez M, Caja S, Melino G, Johnson TS, Lindfors K, Griffin M. A novel extracellular role for tissue transglutaminase in matrix-bound VEGF-mediated angiogenesis. *Cell Death Dis*. 2013;4:e808. doi: 10.1038/cddis.2013.318
16. Kabir-Salmani M, Shiokawa S, Akimoto Y, Sakai K, Sakai K, Iwashita M. Tissue transglutaminase at embryo-maternal interface. *J Clin Endocrinol Metab*. 2005;90:4694–4702. doi: 10.1210/jc.2005-0240
17. Dickneite G, Herwald H, Korte W, Allanore Y, Denton CP, Matucci Cerinic M. Coagulation factor XIII: a multifunctional transglutaminase with clinical potential in a range of conditions. *Thromb Haemost*. 2015;113:686–697. doi: 10.1160/TH14-07-0625
18. Siebenlist KR, Meh DA, Mosesson MW. Protransglutaminase (factor XIII) mediated crosslinking of fibrinogen and fibrin. *Thromb Haemost*. 2001; 86:1221–1228.
19. Procyk R, Blomback B. Factor XIII-induced crosslinking in solutions of fibrinogen and fibronectin. *Biochim Biophys Acta*. 1988;967:304–313.
20. Prince CW, Dickie D, Krumdieck CL. Osteopontin, a substrate for transglutaminase and factor XIII activity. *Biochem Biophys Res Commun*. 1991;177:1205–1210.
21. Lynch GW, Slayter HS, Miller BE, McDonagh J. Characterization of thrombospondin as a substrate for factor XIII transglutaminase. *J Biol Chem*. 1987;262:1772–1778.
22. Tei L, Mazooz G, Shellef Y, Avni R, Vandoorne K, Barge A, Kalchenko V, Dewhirst MW, Chaabane L, Miragoli L, Longo D, Neeman M, Aime S. Novel MRI and fluorescent probes responsive to the Factor XIII transglutaminase activity. *Contrast Media Mol Imaging*. 2010;5:213–222. doi: 10.1002/cmmi.392
23. Mazooz G, Mehlman T, Lai TS, Greenberg CS, Dewhirst MW, Neeman M. Development of magnetic resonance imaging contrast material for *in vivo* mapping of tissue transglutaminase activity. *Cancer Res*. 2005;65:1369–1375. doi: 10.1158/0008-5472.CAN-04-2269
24. Hitomi K, Kitamura M, Sugimura Y. Preferred substrate sequences for transglutaminase 2: screening using a phage-displayed peptide library. *Amino Acids*. 2009;36:619–624. doi: 10.1007/s00726-008-0126-6
25. Piacentini M, Autuori F. Immunohistochemical localization of tissue transglutaminase and Bcl-2 in rat uterine tissues during embryo implantation and post-partum involution. *Differentiation*. 1994;57:51–61.
26. Sugimura Y, Hosono M, Wada F, Yoshimura T, Maki M, Hitomi K. Screening for the preferred substrate sequence of transglutaminase using a phage-displayed peptide library: identification of peptide substrates for TGASE 2 and Factor XIIIA. *J Biol Chem*. 2006;281:17699–17706. doi: 10.1074/jbc.M513538200
27. Sugimura Y, Ueda H, Maki M, Hitomi K. Novel site-specific immobilization of a functional protein using a preferred substrate sequence for transglutaminase 2. *J Biotechnol*. 2007;131:121–127. doi: 10.1016/j.jbiotec.2007.05.037
28. Sugimura Y, Hosono M, Kitamura M, Tsuda T, Yamanishi K, Maki M, Hitomi K. Identification of preferred substrate sequences for transglutaminase 1–development of a novel peptide that can efficiently detect cross-linking enzyme activity in the skin. *FEBS J*. 2008;275:5667–5677. doi: 10.1111/j.1742-4658.2008.06692.x
29. Kawamoto T, Shimizu M. A method for preparing 2- to 50-micron-thick fresh-frozen sections of large samples and undecalcified hard tissues. *Histochem Cell Biol*. 2000;113:331–339.
30. Itoh M, Tatsukawa H, Eun-Seo L, Yamanishi K, Kojima S, Hitomi K. Variations in both TG1 and TG2 isozyme-specific in situ activities and protein expressions during mouse embryonic development. *J Histochem Cytochem*. 2013;61:793–801. doi: 10.1369/0022155413501676

31. Rhee JM, Pirity MK, Lackan CS, Long JZ, Kondoh G, Takeda J, Hadjantonakis AK. In vivo imaging and differential localization of lipid-modified GFP-variant fusions in embryonic stem cells and mice. *Genesis*. 2006;44:202–218. doi: 10.1002/dvg.20203
32. Hsu PD, Scott DA, Weinstein JA, Ran FA, Konermann S, Agarwala V, Li Y, Fine EJ, Wu X, Shalem O, Cradick TJ, Marraffini LA, Bao G, Zhang F. DNA targeting specificity of RNA-guided Cas9 nucleases. *Nat Biotechnol*. 2013;31:827–832. doi: 10.1038/nbt.2647
33. Doench JG, Hartenian E, Graham DB, Tothova Z, Hegde M, Smith I, Sullender M, Ebert BL, Xavier RJ, Root DE. Rational design of highly active sgRNAs for CRISPR-Cas9-mediated gene inactivation. *Nat Biotechnol*. 2014;32:1262–1267. doi: 10.1038/nbt.3026
34. Doench JG, Fusi N, Sullender M, Hegde M, Vaimberg EW, Donovan KF, Smith I, Tothova Z, Wilen C, Orchard R, Virgin HW, Listgarten J, Root DE. Optimized sgRNA design to maximize activity and minimize off-target effects of CRISPR-Cas9. *Nat Biotechnol*. 2016;32:184–191. doi:10.1038/nbt.3437.
35. Xu H, Xiao T, Chen CH, Li W, Meyer CA, Wu Q, Wu D, Cong L, Zhang F, Liu JS, Brown M, Liu XS. Sequence determinants of improved CRISPR sgRNA design. *Genome Res*. 2015;25:1147–1157. doi: 10.1101/gr.191452.115
36. Chari R, Mali P, Moosburner M, Church GM. Unraveling CRISPR-Cas9 genome engineering parameters via a library-on-library approach. *Nat Methods*. 2015;12:823–826. doi: 10.1038/nmeth.3473
37. Sanjana NE, Shalem O, Zhang F. Improved vectors and genome-wide libraries for CRISPR screening. *Nat Methods*. 2014;11:783–784. doi: 10.1038/nmeth.3047
38. Regev L, Neufeld-Cohen A, Tsoory M, Kuperman Y, Getselter D, Gil S, Chen A. Prolonged and site-specific over-expression of corticotropin-releasing factor reveals differential roles for extended amygdala nuclei in emotional regulation. *Mol Psychiatry*. 2011;16:714–728. doi: 10.1038/mp.2010.64
39. Kumasawa K, Ikawa M, Kidoya H, Hasuwa H, Saito-Fujita T, Morioka Y, Takakura N, Kimura T, Okabe M. Pravastatin induces placental growth factor (PGF) and ameliorates preeclampsia in a mouse model. *Proc Natl Acad Sci USA*. 2011;108:1451–1455. doi: 10.1073/pnas.1011293108
40. Plaks V, Kalchenko V, Dekel N, Neeman M. MRI analysis of angiogenesis during mouse embryo implantation. *Magn Reson Med*. 2006;55:1013–1022. doi: 10.1002/mrm.20881
41. Plaks V, Gershon E, Zeisel A, Jacob-Hirsch J, Neeman M, Winterhager E, Rechavi G, Domany E, Dekel N. Blastocyst implantation failure relates to impaired translational machinery gene expression. *Reproduction*. 2014;148:87–98. doi: 10.1530/REP-13–0395
42. Dafni H, Gilead A, Nevo N, Eilam R, Harmelin A, Neeman M. Modulation of the pharmacokinetics of macromolecular contrast material by avidin chase: MRI, optical, and inductively coupled plasma mass spectrometry tracking of triply labeled albumin. *Magn Reson Med*. 2003;50:904–914. doi: 10.1002/mrm.10638
43. Ádány R, Bárdos H, Antal M, Módis L, Sárváry A, Szücs S, Balogh I. Factor XIII of blood coagulation as a nuclear crosslinking enzyme. *Thromb Haemost*. 2001;85:845–851. doi:10.1055/s-0037-1615758
44. Pulendran B, Smith JL, Caspary G, Brasel K, Pettit D, Maraskovsky E, Maliszewski CR. Distinct dendritic cell subsets differentially regulate the class of immune response in vivo. *Proc Natl Acad Sci USA*. 1999;96:1036–1041. doi: 10.1073/pnas.96.3.1036
45. Asahina T, Kobayashi T, Okada Y, Itoh M, Yamashita M, Inamato Y, Terao T. Studies on the role of adhesive proteins in maintaining pregnancy. *Horm Res*. 1998;50 (suppl 2):37–45. doi: 10.1159/000053122
46. Di Simone N, Silano M, Castellani R, Di Nicuolo F, D'Alessio MC, Franceschi F, Tritarelli A, Leone AM, Tersigni C, Gasbarrini G, Silveri NG, Caruso A, Gasbarrini A. Anti-tissue transglutaminase antibodies from celiac patients are responsible for trophoblast damage via apoptosis in vitro. *Am J Gastroenterol*. 2010;105:2254–2261. doi: 10.1038/ ajg.2010.233
47. Dorgalaleh A, Rashidpanah J. Blood coagulation factor XIII and factor XIII deficiency. *Blood Rev*. 2016;30:461–475. doi: 10.1016/j.blre.2016.06.002